Lipid composition affects the thermal stability of cytochrome P450 3A4 in nanodiscs

Knetsch, T.G.J.; Ubbink, M.

BBA - Biomembranes 1866 (2024) 184372

Contents lists available at ScienceDirect

BBA - Biomembranes

journal homepage: www.elsevier.com/locate/bbamem

Lipid composition affects the thermal stability of cytochrome P450 3A4 in nanodiscs

Tim G.J. Knetsch, Marcellus Ubbink*

Leiden Institute of Chemistry, Leiden University, Einsteinweg 55, 2333 CC Leiden, the Netherlands

ARTICLE INFO

Keywords:
Nanodiscs
Cytochrome P450
Lipid composition
Thermal stability
Multi-angle light scattering

ABSTRACT

Nanodiscs (NDs), self-assembled lipid bilayers encircled by membrane scaffold proteins (MSPs), offer a versatile platform for the reconstitution of membrane proteins for structural and biochemical investigations. Saturated, isoprenoid lipids are commonly found in thermophiles and have been associated with thermotolerance. To test whether these lipids confer additional stability on ND-incorporated membrane proteins, this study focuses on the thermal stability of human cytochrome P450 3A4 (CYP3A4) inside NDs composed of different phosphocholine lipids: 1-palmitoyl-2-oleoyl-sn-glycero-3-phosphocholine (POPC), 1,2-dimyristoyl-sn-glycero-3-phosphocholine (DMPC), and 1,2-diphytanoyl-sn-glycero-3-phosphocholine (DPhPC). NDs were characterized using size-exclusion chromatography coupled with multi-angle light scattering (SEC-MALS) and densitometric SDS-PAGE. CYP3A4-DPhPC-NDs were found to comprise three MSP copies instead of the canonical dimer, as reported before for the empty NDs. Rapid, thermally induced unfolding of CYP3A4 inside NDs measured using circular dichroism and differential scanning fluorimetry (nanoDSF) revealed that the CYP3A4 melting temperature was dependent on ND composition. In POPC and DMPC-CYP3A4-NDs the melting temperature was comparable to CYP3A4 without NDs (59 °C). CYP3A4 in DPhPC-NDs showed an increase in melting temperature of 4 °C. Decline in CYP3A4 integrity as well as ND aggregation and disintegration occur at similar rates for all membrane types when subjected to exposure at 37 °C for several hours. The POPC and DMPC- CYP3A4-NDs show significant lipid loss over time, which is not observed for DPhPC-NDs. The results demonstrate that thermally induced denaturation of protein-NDs is a complex, multifaceted process, which is not represented well by rapid thermal unfolding experiments.

1. Introduction

Apolipoprotein A1 (ApoA1), the predominant constituent in high-density lipoprotein (HDL) of the human reverse cholesterol transport pathway, has the capacity to bind lipids and form discoidal particles stable in solution [1,2]. From ApoA1, membrane scaffold proteins (MSPs) have been derived, comprising solely the lipid-binding helical-repeat domains of ApoA1. They similarly wrap around the hydrophobic alkyl chains of lipids in a belt-like fashion to form nanometre-sized protein-lipid Nanodiscs (NDs) [3,4]. NDs provide a platform for the reconstitution of membrane proteins of interest for structural and biophysical studies, and have been extensively reviewed [5–10]. NDs, with their ability to mimic the lipid environment of biological membranes, have emerged as a valuable tool for studying enzymes in a monomeric state. Here, we used cytochrome P450 3A4 (CYP3A4) to study the integrity and stability of a membrane protein in NDs. CYP3A4 is advantageous as a model protein because the haem prosthetic group allows independent evaluation of thermal stability of the membrane protein inside NDs. CYPs are found in the human liver and intestinal tract, where they reside primarily in the endoplasmic reticulum membrane [11], and have a major role in biotransformation of both endogenous ligands, such as in steroid biosynthesis, and the breakdown of xenobiotics. It has been predicted that CYPs are involved in ~75 % of metabolism of all marketed drugs, with CYP3A4 being the most prevalent human isoform [12,13]. CYPs are haem-thiolate proteins that catalyse mono-oxygenase reactions. Their involvement in the metabolism of a diverse range pharmacologically active substances found in food and medicine makes them susceptible to inhibition or activation by concomitant drug administration [14]. CYPs are attached to the membrane via a single transmembrane helix, and are able to cruise over the membrane surface while being partially submerged [13,15–17]. The CYP3A4 active site haem can be reached with the help of a network of

* Corresponding author.
E-mail address: m.ubbink@chem.leidenuniv.nl (M. Ubbink).

https://doi.org/10.1016/j.bbamem.2024.184372
Received 6 April 2024; Received in revised form 20 June 2024; Accepted 16 July 2024
Available online 22 July 2024

access/egress channels from/to both the aqueous and membrane environments to enable interactions with a range of substrates and products that differ in hydrophobicity. Thermal stability of CYP is highly dependent on single nucleotide polymorphisms (SNPs), and exposure to elevated temperatures leads to conversion to the so-called P420 form (loss of iron coordination of the axial cysteine ligand) and a concomitant decrease in activity [18–21]. NDs have been used to study these enzymes in a monomeric state, helping to the elucidate mechanisms of the homo/heterotropic cooperative substrate binding, accommodated by the spacious active site of CYP3A4 [22–25].

The mono-unsaturated lipid 1-palmitoyl-2-oleoyl-sn-glycero-3-phosphocholine (POPC, 16:0–18:1) has a main lipid phase transition temperature (T_m) of −2 °C in liposomes and is the most commonly used lipid for reconstitution of P450 enzymes at low temperatures. The thermal stability of CYP3A4-POPC- NDs has been investigated using differential scanning calorimetry (DSC) [16]. In this study a higher thermal stability was reported for CYP3A4 inside NDs than in solution, in which CYP3A4 is in an aggregated state. The fully saturated lipid 1,2-dimyristoyl-sn-glycero-3-phosphocholine (DMPC, 14:0, T_m = 24 °C) was also employed in an earlier study by McClary and coworkers to investigate the effect of mixed membranes of POPC and DMPC on CYP3A4 thermal stability using DSC and circular dichroism (CD) spectroscopy [26]. It was reported that CYP3A4 thermal stability improved with an increasing fraction of DMPC, with an optimum at 50 % DMPC.

Previously, we have compared the thermal stability of empty NDs comprising different phosphocholine lipids. NDs were prepared with lipids that differ in saturation, have either ether- or ester linkages between the fatty acid and glycerol backbone or contain isoprenoid fatty acid tails [27]. Fully saturated lipids such as dipalmitoylphosphatidylcholine (DPPC, 16:0) produced the most thermostable NDs. However, DPPC membranes have a high T_m of 41 °C, which is detrimental for the incorporation of CYP3A4 and, therefore, was not used in this study. 1,2-Diphytanoyl-sn-glycero-3-phosphocholine (DPhPC, 16:0, 4ME) has unique properties stemming from its saturated isoprenoid lipid tails. DPhPC membranes display no measurable temperature transition between −120 and + 120 °C and their NDs deviate from classic NDs by comprising a third copy of the MSP instead of the canonical dimer [27]. Isoprenoid alkyl chains lipids are commonly found in the membranes of thermophilic Archaea and have been associated with thermotolerance [28,29]. Here, POPC, DMPC and DPhPC lipids (Fig. 1) were selected to prepare NDs, incorporate CYP3A4 and test if the stabilizing effect of the lipids on 'empty' NDs can be translated to a membrane protein-incorporated ND.

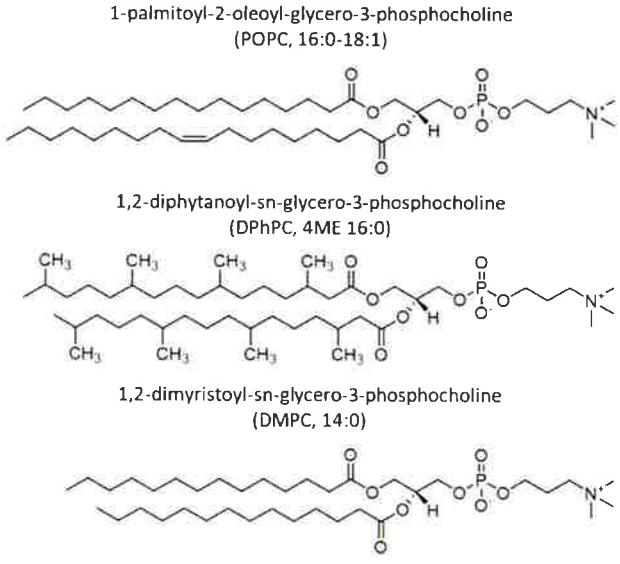

Fig. 1. Chemical structures of the phospholipids used for ND assembly.

Self-assembled molecular systems such as NDs comprise multiple components, and inherently form heterogeneous particles. NDs have a size limit determined by maximum number of lipids that can be confined by the MSP belt. However, smaller products than the maximally loaded configuration are much more likely and can be considered the rule rather than the exception [30]. Unfortunately, the self-assembly process is not well understood, but critically depends on the stoichiometry of the components, which have to be laboriously optimized. When a target membrane protein is introduced, and alongside it, co-purified lipids and detergent, heterogeneity can increase. Particles surpassing the theoretical size of a protein-ND with one protein molecule could be carrying multiple copies of the protein or consist of an aggregate. Such species may nevertheless contain functional membrane protein, but depending on the downstream application could be deleterious. Even within a single, well-resolved size exclusion chromatography (SEC) peak, a distribution of the assembly components is often found. We and others [27,31–33] have shown that the lipid component decreases steadily across the elution peak, meaning that the trailing end of the peak represents NDs with fewer lipids than the NDs at the front of the peak. To obtain a sample that is as monodisperse as possible, a trade-off has to be made between yield and homogeneity. Thus, it is of importance to visualize the underlying particle distributions to optimize the assembly procedure towards a desired composition. In this paper we address ND size distributions encountered after a typical ND reconstitution experiment, next we determine the molecular weight (Mw) of the particle populations and their composition through densitometric and SEC-MALS protein-conjugate analysis. Our main objective is to investigate the effect of lipid composition on the formation and thermostability of protein-NDs complexes and establish whether ND lipid composition can extend the lifetime of an incorporated target membrane protein.

Interestingly, CYP3A4-DPhPC-NDs were shown to contain three copies of the scaffold protein instead of the canonical dimer of MSP, in line with what was observed in our prior research on empty DPhPC-NDs [27]. In CYP3A4-NDs formed with POPC and DMPC, the melting temperature closely resembled that of CYP3A4 in solution, whereas CYP3A4 in DPhPC-NDs exhibited a significant increase in melting temperature. However, this stabilization does not translate to a longer lifetime when exposed for several hours to 37 °C, which leads to a decline in CYP3A4 integrity as well as aggregation and disintegration of NDs. During such incubations, lipid loss is observed for POPC and DMPC-NDs but not for DPhPC-NDs.

2. Results

2.1. CYP3A4-NDs assembled with DPhPC contain three copies of MSP1D1

NDs were prepared by dissolution of dry lipid into aqueous buffer containing cholate detergent, MSP1D1 and CYP3A4 labelled with a His-tag. Self-assembly of NDs was initiated by removal of detergent through dialysis at the lipid phase transition temperature. The resulting mixture was applied to an immobilized metal affinity chromatography (IMAC) column to remove empty NDs, followed by size-exclusion chromatography (SEC). Analytical SEC coupled to multi-angle light scattering (SEC-MALS) and densitometric SDS-PAGE were used to characterize the SEC fractions expected to contain the NDs to determine the weight fractions of CYP3A4-ND components. Empty NDs assembled with DPhPC lipids comprise three copies of the scaffold protein [27], raising the question whether a third copy of MSP1D1 is also present in CYP3A4-NDs. The data show that CYP3A4-DPhPC-NDs have a size of ~190 kDa and comprise three copies of MSP1D1 as determined by densitometric SDS-PAGE, and mostly contain one copy of CYP3A4, as was measured by SEC-MALS (Fig. 2). Another species of ~240 kDa was identified which contains two CYP3A4 copies (Table 1). It is difficult to fully resolve these

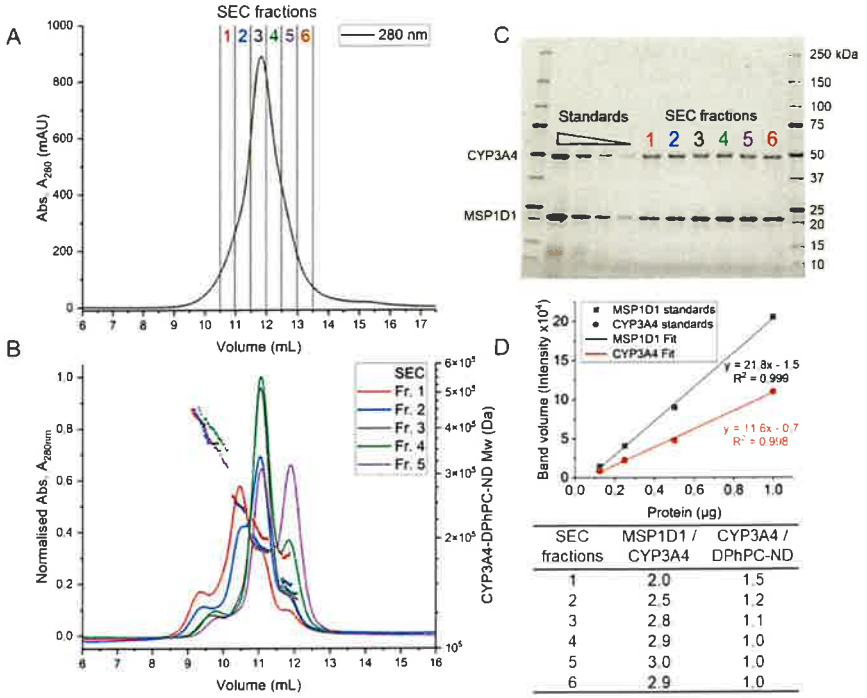

SEC fractions	MSP1D1 / CYP3A4	CYP3A4 / DPhPC-ND
1	2.0	1.5
2	2.5	1.2
3	2.8	1.1
4	2.9	1.0
5	3.0	1.0
6	2.9	1.0

Fig. 2. Characterization of CYP3A4-DPhPC-NDs size and composition. (A) After self-assembly, NDs were purified by IMAC to remove empty NDs, followed by preparative SEC, absorbance was monitored at 280 nm. (B) The underlying particle populations of the initial SEC experiment shown in A were further resolved by reinjection of the numbered fractions on a SEC-MALS system. The total Mw of the CYP3A4-DPhPC-NDs is shown in the SEC-MALS chromatogram. The Mw of CYP3A4 and of the ND conjugate ($Mw_{Nanodisc}$, MSP + lipids), were determined by protein conjugate analysis around the peak maxima, using the 417 nm absorbance to quantify CYP3A4. All fractional Mw data are summarized in Table 1. (C) The ratios of MSP1D1 and CYP3A4 were measured by densitometric SDS-PAGE for each fraction. The relative band intensity was quantified by comparing to MSP1D1 and CYP3A4 standards of known concentrations. (D) The linear relationship between band intensity and amount of protein was used to calculate the molar ratio between the components. As can be seen from the table in D, CYP3A4-DPhPC-NDs contain three copies of MSP1D1 per ND, instead of the canonical dimer, as was previously determined for DPhPC-NDs without an inserted protein [27]. Due to the presence of higher Mw species, determined by SEC-MALS to contain two copies of CYP3A4 (~10.5 mL), early fractions show a lower average MSP1D1 / CYP3A4.

Table 1
Size and composition of CYP3A4-DPhPC-ND fractions in Fig. 2, measured at peak maxima by SEC-MALS protein-conjugate analysis. The expected size for CYP3A4-DPhPC-NDs was calculated by assuming three copies of MSP1D1, one copy of CYP3A4 and 24–30 DPhPC lipids per MSP1D1 [27]. The expected Mw_{CYP3A4} was calculated from the amino acid sequence, with the addition of haem *b*. The 1st SEC fraction contained a mixture of NDs with one or two copies of CYP3A4, producing an Mw_{CYP3A4} of ~100 kDa at the apex of the peak.

SEC fractions	$Mw_{CYP3A4\text{-}ND}$ (kDa)[a]	Mw_{CYP3A4} (kDa)[b]	$Mw_{Nanodisc}$ (kDa)[c]	Mw_{Lipid} (kDa)[d]	Lipids/nanodisc	Lipids/MSP1D1
Expected size	193 ± 7	59	135 ± 7	68 ± 8	81 ± 9	27 ± 3
Fr. 1	248	103	145	79	93	31
Fr. 2	192	63	129	63	74	25
Fr. 3	191	60	130	64	76	25
Fr. 4	186	58	128	62	73	24
Fr. 5	188	62	126	60	71	24

[a] $Mw_{CYP3A4\text{-}ND}$ is the size of the entire CYP3A4-ND complex calculated using the A_{417nm} and dRI signals to determine the concentration for the light scattering calculations.
[b] Mw_{CYP3A4} was determined using the A_{417nm} to determine the concentration of CYP3A4 for the light scattering calculations.
[c] $Mw_{Nanodisc}$ is the calculated weight fraction of the conjugated ND, after subtraction of Mw_{CYP3A4} from $Mw_{CYP3A4\text{-}ND}$.
[d] Mw_{Lipid} was calculated by subtracting three copies of $Mw_{MSP1D1(-his)}$ (3 × 22 kDa) from $Mw_{Nanodisc}$.

NDs, so an average Mw of NDs is obtained for the overlapping peaks. However, the measured weights are in close agreement with the expected values based on the Mw of CYP3A4 and empty DPhPC-NDs. The Mw of CYP3A4 was measured directly by protein-conjugate analysis using the absorbance at 417 nm from the haem Soret band to determine the concentration for the light scattering calculations. For proteins lacking an absorbance band other than the one at 280 nm, it is difficult to distinguish between MSP and target membrane protein. In that case a densitometric analysis is especially useful to supplement the SEC-MALS protein-conjugate analysis.

2.2. CYP3A4 is thermostabilized in DPhPC NDs

CYP3A4-NDs comprising POPC, DPhPC or DMPC were freshly purified for a comparison of thermal stability of CYP3A4 inside NDs with different lipid compositions. Interestingly, the highest yield of CYP3A4-NDs was obtained by reconstitution with DPhPC, followed by POPC and DMPC lipids, suggesting that DPhPC is suited for the reconstitution of membrane proteins that are not natively present in isoprenoid membranes. It was also apparent from the SEC purification after self-assembly (Fig. 3) that formation of CYP3A4-DMPC-NDs does not efficiently take place at 25 °C and yields heterogeneous particles, because a

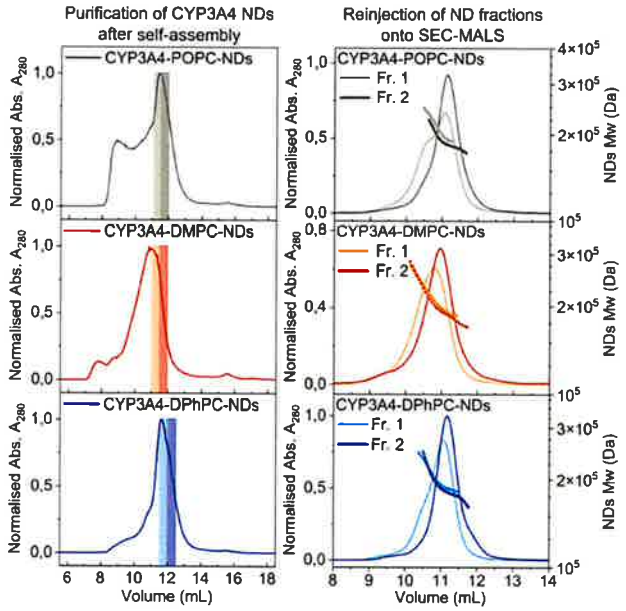

Fig. 3. SEC purifications of CYP3A4-NDs prepared with POPC, DMPC or DPhPC lipids after self-assembly are shown on the left (empty NDs were removed prior to SEC by IMAC). The highlighted area depicts the ND fractions that were reinjected on an SEC-MALS system (chromatograms on the right). The Mw of the entire CYP3A4-ND complex are shown, the CYP3A4 and lipid weight fractions can be found in Table 2. Note the Mw plateauing at the peak apex (~200 kDa) and the larger Mw of the two-copy CYP3A4-NDs (~250 kDa) and aggregates species (> 250 kDa) to the left of the main ND peak. The NDs in the 2nd fractions (darker colours) are more homogeneous.

broad elution peak and aggregates are present.

Nevertheless, CYP3A4-DMPC-NDs could be isolated as confirmed by SEC-MALS (Fig. 3), and the sizes and composition of all freshly purified CYP3A4-NDs are summarised in Table 2. The SEC calibration standard curve for the initial ND purification is shown in Fig. S1. Note the left shoulder peak around 10.5 mL elution volume for CYP3A4-POPC-NDs and CYP3A4-DPhPC-NDs, which contain two copies of CYP3A4.

To investigate the thermal stability of CYP3A4 inside different lipid membranes, CD spectroscopy and differential scanning fluorimetry (nanoDSF) measurements were employed. CD provides a measure of the unfolding of proteins as a function of temperature. From the midpoint of the unfolding transition, the protein melting temperature (T_m) is derived. Proteins like CYP3A4 and MSP1D1, which are largely alpha helical, display characteristic minima at 208 and 222 nm. For an aggregate of CYP3A4 in the absence of detergent, the loss of CD signal at 222 nm was measured between 20 and 95 °C (Fig. 4). A clear unfolding transition was observed with a T_m of 59.6 ± 0.1 °C, which was reproducible between different batches of purified protein and is similar to what has been reported in literature [34]. The steep slope of the unfolding transition is indicative of positive cooperative unfolding of the aggregated CYP3A4. The same temperature scan was performed for empty POPC, DMPC and DPhPC-NDs to measure the change in residue ellipticity at 222 nm originating from the ND scaffold proteins (Fig. 5.). Unfolding of MSP1D1 in empty POPC and DMPC-NDs was very comparable, however, for DPhPC-NDs the onset of the unfolding transition happens earlier. At the same ND concentration, the mean residue ellipticity of DPhPC-NDs MSPs was exactly 1.5 times that of POPC and DMPC-NDs, in line with the presence of a third copy of MSP in these NDs and suggesting that the MSPs have a comparable α-helical fold at 20 °C. The reason for an earlier onset of unfolding is unclear, but may be related to the presence of three MSP copies in DPhPC-NDs. The unfolding transition for empty NDs is incomplete, therefore T_m values were not determined, but these are estimated to be above 75 °C. To determine the T_m for CYP3A4 in NDs, the background change in ellipticity of the empty NDs was subtracted from the CD temperature scan of the CYP3A4-NDs, yielding T_m values of 58.7 ± 0.3, 58.3 ± 0.3 and 62.4

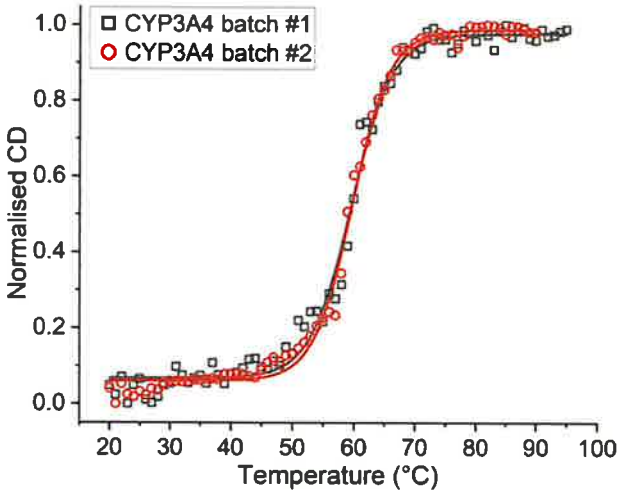

Fig. 4. CD spectroscopy temperature scan for CYP3A4 in solution without detergent from two purification batches. The average melting temperature, T_m, is 59.6 ± 0.1. °C.

Table 2
Size and composition of CYP3A4-NDs assembled with POPC, DPhPC and DMPC lipids measured by SEC-MALS, averages of five replicate measurements are shown ± two standard deviations of the mean.

CYP3A4-NDs containing	$Mw_{CYP3A4\text{-}ND}$ (kDa)[a]	Mw_{CYP3A4} (kDa)[b]	$Mw_{Nanodisc}$ (kDa)[c]	Mw_{Lipid} (kDa)[d]	Lipids/nanodisc	Lipids/MSP1D1
POPC Expected	198	59	140	96[e]	126	63
POPC, Fr. 1	197 ± 1	60 ± 0.8	136 ± 0.8	92 ± 0.8	121 ± 1	61 ± 1
POPC, Fr. 2	186 ± 1	60 ± 0.8	127 ± 0.8	83 ± 0.8	109 ± 1	55 ± 1
DMPC Expected	208	59	150	106[e]	156	78
DMPC, Fr. 1	210 ± 5	58 ± 3	153 ± 5	109 ± 5	160 ± 8	80 ± 4
DMPC, Fr. 2	195 ± 5	53 ± 3	142 ± 5	98 ± 5	144 ± 8	72 ± 4
DPhPC Expected	193	59	135	68[e]	81	27
DPhPC, Fr. 1	193 ± 2	58 ± 2	134 ± 2	68 ± 2	80 ± 3	27 ± 1
DPhPC, Fr. 2	181 ± 2	57 ± 2	124 ± 2	58 ± 2	68 ± 3	23 ± 1

[a] $Mw_{CYP3A4\text{-}ND}$ is the size of the entire CYP3A4-ND complex calculated using the A_{417nm} and dRI signals to determine the concentration for the light scattering calculations.
[b] Mw_{CYP3A4} was determined using the A_{417nm} to determine the concentration of CYP3A4 for the light scattering calculations.
[c] $Mw_{Nanodisc}$ is the weight fraction of the conjugated ND, after subtraction of Mw_{CYP3A4} from $Mw_{CYP3A4\text{-}ND}$.
[d] Mw_{Lipid} was calculated by subtracting three copies of $Mw_{MSP1D1(\ his)}$ (3 × 22 kDa) from $Mw_{Nanodisc}$.
[e] The expected Mw_{Lipid} is based on empty ND composition with 4 lipids displaced by CYP3A4 membrane helix per ND.

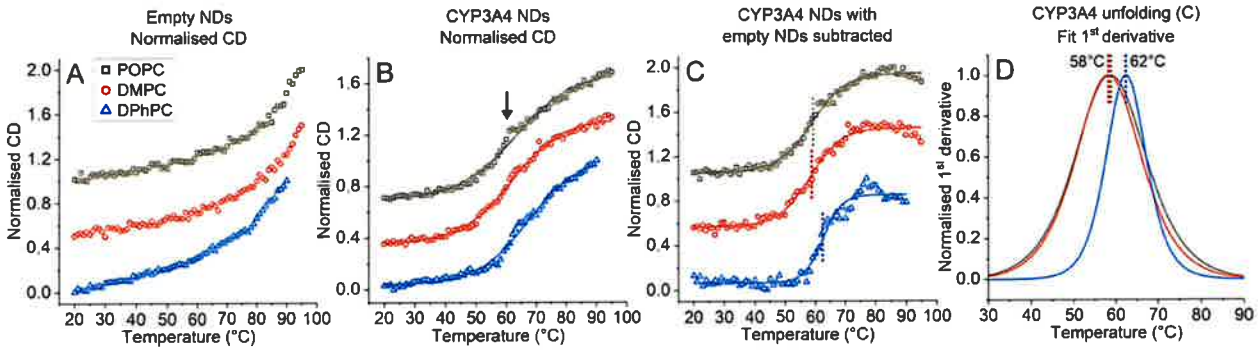

Fig. 5. CD spectroscopy temperature scan for empty (lipid-only) and CYP3A4-NDs comprising POPC (black squares), DMPC (red circles) and DPhPC (blue triangles) lipids. (A) The MSP inside empty NDs does not display complete unfolding over the measured temperature range. (B) The unfolding transition of CYP3A4 in NDs is the summation of the effects on the MSP and CYP3A4. The arrow indicates where the unfolding of CYP3A4 is clearly visible. (C) Subtraction of the CD signal from the respective empty NDs yields the curves for CYP3A4 unfolding inside NDs. Sigmoidal fits are represented by the solid lines and T_m's are indicated by the vertical dotted lines, and listed in Table 3. (D) The 1st derivatives of the unfolding transition fits show a ~ 4 °C higher T_m for CYP3A4 in DPhPC NDs than in POPC or DMPC NDs. The CD curves for DMPC and POPC samples are displaced vertically for clarity.

± 0.4 °C for POPC, DMPC and DPhPC-CYP3A4-NDs, respectively.

NanoDSF measures the fluorescence intensity ratio at 350 / 330 nm of intrinsic tryptophan and tyrosine residues in MSP1D1 and CYP3A4, which become solvent exposed upon unfolding. Thermally induced unfolding curves of CYP3A4 in solution without detergent measured by nanoDSF closely resemble the CD data, showing a single T_m at 59.3 ± 0.3 (Fig. 6). Similar to the CD analysis, for CYP3A4-NDs, the contribution of the empty NDs to the total fluorescence intensity ratio was subtracted (Fig. 7). The two methods yield very similar results (Table 3) and show that CYP3A4 in POPC- and DMPC-NDs has a melting temperature similar or slight less than in solution. In the DPhPC-ND, CYP3A4 is thermostabilized by 3–4 °C.

2.3. POPC and DMPC but not DPhPC NDs lose lipids over time

We wondered whether the rapid thermal denaturation measured by CD and nanoDSF is a suitable predictor of stability during prolonged exposure to moderate temperatures. The long-term stability of NDs at such temperatures is of interest for their application in drug screening and formulation. The human body temperature is the most relevant for CYP3A4 biology, and for the potential application of NDs as a carrier–/drug delivery system. Thus, the long-term stability of CYP3A4-NDs formed with POPC, DMPC and DPhPC were compared at 37 °C. The integrity of CYP3A4 haem active site was measured by carbon monoxide binding after 5–168 h (one week) at 37 °C. When the axial cysteine sulphur ligand is bound to the haem iron, a characteristic maximum of the Soret band is observed for the ferrous CO-bound enzyme at 450 nm. Upon loss of the axial ligand, a band at 420 nm is visible, indicative of

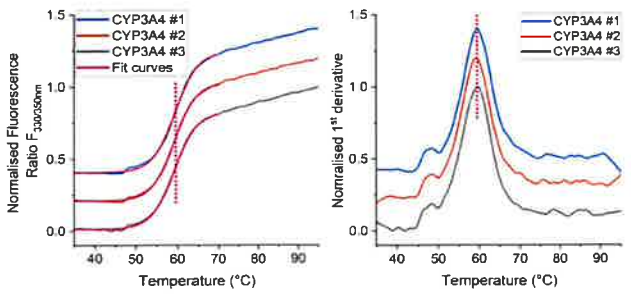

Fig. 6. NanoDSF temperature scan for CYP3A4 in solution without detergent for three batches. The average T_m = 59.3 ± 0.3 °C. The POPC and DMPC curves are displaced vertically for clarity. Left, normalised Fluorescence; right, 1st derivative.

inactive CYP3A4 [18,19]. Before incubation at 37 °C, CYP3A4-NDs showed a fraction of ~95 % of active enzyme for POPC and DPhPC-NDs and ~ 90 % for CYP3A4-DMPC-NDs. The somewhat lower active fraction of CYP3A4 in DMPC-NDs can probably be attributed to the required 48 h of dialysis at 25 °C during ND assembly, which is the approximate T_m of DMPC membranes. The active fractions of CYP3A4 were normalised to 100 % at the start of the analysis for comparison between the different NDs and CO binding spectra were measured over time (Fig. 8). The data show a clear decrease in CYP3A4 integrity for all NDs. The decline in POPC- and DPhPC-NDs was comparable, whereas CYP3A4 showed a faster integrity loss in DMPC-NDs. Control samples measured after one week at 4 °C show that all CYP3A4-NDs were mostly unaffected by storage at this temperature. To establish the size distribution of NDs and aggregates, the same samples were subjected to analytical SEC. The elution profiles were deconvoluted to determine the peak surface area of the NDs with a single copy of CYP3A4 at the start, and during exposure at 37 °C (Fig. 9). Elution profiles are reported for the three types of CYP3A4-NDs, and the relative recovery of the CYP3A4-ND area under the curves are summarized in the bottom right panel of Fig. 10. The data show that CYP3A4-NDs disintegrate at 37 °C over the course of several hours to several days. CYP3A4-DMPC-NDs were the least stable, showing a rapid decrease in peak area after just 5 h of incubation at 37 °C. CYP3A4-DPhPC-NDs initially appear the most stable, before decreasing faster after 24 h than CYP3A4-POPC-ND, which was the most stable after 48 h – 1 week of exposure. A difference in the degree of aggregation is observed between CYP3A4-NDs containing POPC and CYP3A4-NDs prepared with DMPC or DPhPC. The distribution of aggregated species should be interpreted with care because these are large, ill-defined particles that could also be partially lost on the HPLC or column filters before reaching the detectors. For the CYP3A4-NDs formed with POPC and DMPC, a shift of the main peak to a later elution volume is apparent, a phenomenon we observed previously for empty NDs, and that was attributed to a loss of lipids, and not MSP1D1 [27]. If the size differences measured by SEC-MALS for CYP3A4-NDs are attributed to the lipid component, this translates to a ~ 5 % and ~ 10 % loss of POPC and DMPC lipids, respectively after 72 h, and ~ 20 % loss of POPC lipids after one week. The CYP3A4-DPhPC-NDs do not display a shift in elution volume and concomitant loss of lipid. For CYP3A4-POPC-NDs a peak at 10.5 mL remains visible, which corresponds roughly to the size of a ND with two copies of CYP3A4 and this species is equally stable as the monomeric CYP3A4-POPC-NDs. Due to more overlap with variable aggregated species in this region, the quantification of NDs with two copies of CYP3A4 is not possible for DPhPC and DMPC. Smaller species are also present at ~16 mL elution volume, corresponding to the expected size of MSP1D1 devoid of lipid.

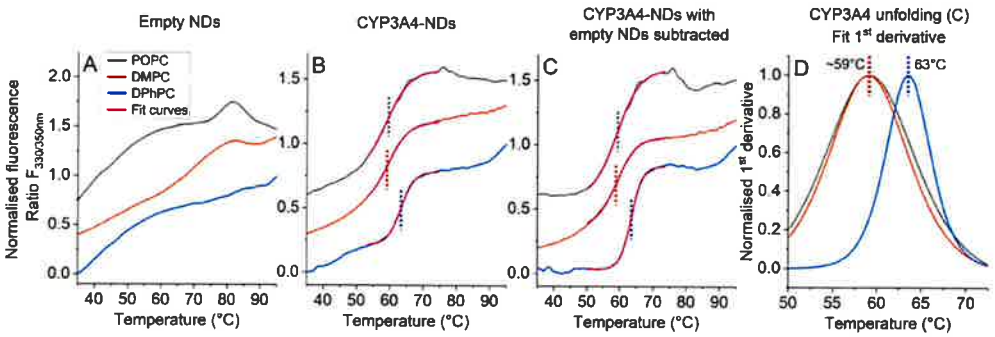

Fig. 7. Thermally induced unfolding of empty - (A) and CYP3A4 NDs (B), comprising POPC, DPhPC and DMPC lipids, measured by differential fluorescence. (C) Subtraction of the empty ND fluorescence signal yields similar T_m values for CYP3A4 in NDs. Data were analysed by performing a Boltzmann fit (magenta lines) over the 50–75 °C region encompassing the main T_m of CYP3A4 in NDs (dotted lines). (D) The 1st derivatives of the unfolding transition fits show a ~ 4 °C higher T_m for CYP3A4 in DPhPC NDs than in POPC or DMPC NDs. The POPC and DMPC fluorescence intensity ratio curves are displaced vertically for clarity.

Table 3
CD and differential fluorescence T_m values for CYP3A4 in solution without detergent and inside NDs. The contributions of MSP1D1 to the CD helicity or NanoDSF fluorescence intensity ratio in the empty NDs were subtracted from CYP3A4-NDs.

Sample	CD, T_m (°C)	NanoDSF, T_m (°C)
CYP3A4 in buffer	59.7 ± 0.1[a]	59.3 ± 0.3 [c]
CYP3A4-POPC-NDs	58.7 ± 0.3[b]	59.2 ± 0.1[c]
CYP3A4-DMPC-NDs	58.3 ± 0.3[b]	58.4 ± 0.9[c]
CYP3A4-DPhPC-NDs	62.4 ± 0.4[b]	63.2 ± 0.9[c]

[a] Average of two measurements ± two standard deviations of the mean.
[b] Standard error of the mean of the sigmoidal fit.
[c] Averages of 3 to 6 measurements ± two standard deviations of the mean.

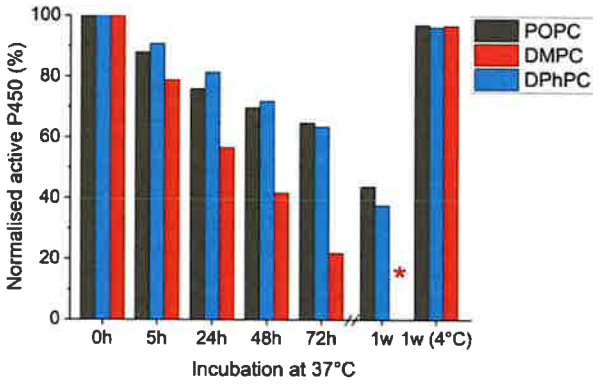

Fig. 8. Active fraction of CYP3A4 in NDs based on carbon monoxide binding, for NDs containing POPC, DPhPC and DMPC. The red asterisk indicates missing data.

The normalised absorbance ratio was calculated from the deconvoluted peak areas measured at 417 nm (CYP3A4) and 280 nm (CYP3A4 + MSP1D1) for the main peak CYP3A4-NDs. A ratio of 1 indicates that CYP3A4 remains present inside the ND. The $A_{417nm/280nm}$ ratio minimally decreases to ~0.9, indicating some loss of CYP3A4 or haem cofactor but the majority remains NDs encapsulated during the temperature incubation, though much of the CYP3A4 becomes inactivated as seen by the appearance of 420 nm band in the carbon monoxide assay.

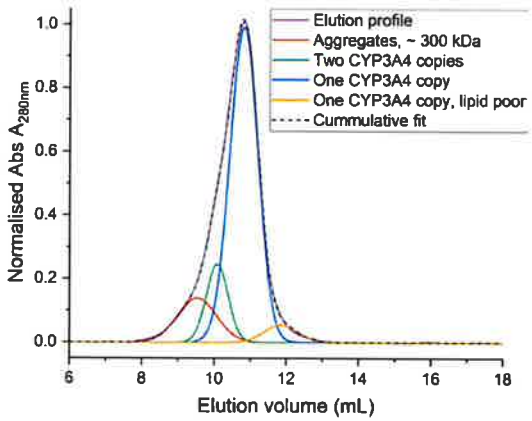

Fig. 9. Deconvolution and fitting of CYP3A4-DMPC-NDs elution profile with a sum of gaussians.

3. Discussion and conclusions

3.1. Discusssion

NDs self-assembled with DPhPC were shown to contain three copies of MSP1D1 in the absence [27] and presence of incorporated CYP3A4. This observation suggests that the lipid membrane is an important driving force of ND formation and that ND topology can be influenced through self-assembly by changing the lipid composition. The detailed organisation of MSPs in DPhPC-NDs remains unclear and is a subject of future research. Thermally induced unfolding of CYP3A4-ND was assessed through CD, nanoDSF and SEC-MALS, aimed at monitoring different aspects of stability. The rapid temperature ramp experiments yielded a T_m of ~59–64 °C for CYP3A4, and CYP3A4-ND integrity was measured after prolonged exposure at 37 °C, where aggregation and disintegration of NDs are evident over time. Previously, McClary and coworkers reported a lower T_m of ~50 °C for CYP3A4 in aqueous solution without detergent and the enzyme was thermostabilized by incorporation into NDs, yielding a T_m of ~56 °C [16,26]. However, the CD thermal unfolding measurements were not adjusted for the helicity of MSP1D1. Interestingly, an increase in the T_m of CYP3A4 inside NDs comprising POPC/DMPC mixtures, with an optimum at 50 % DMPC, was also reported. Lipid mixtures were beyond of the scope of this study, because it is not trivial to distinguish between lipid mixtures inside NDs after assembly, let alone monitor lipid composition during the course of a temperature-dependent experiment. Mixed lipid NDs composition could also display significant disc-to-disc variation while having similar

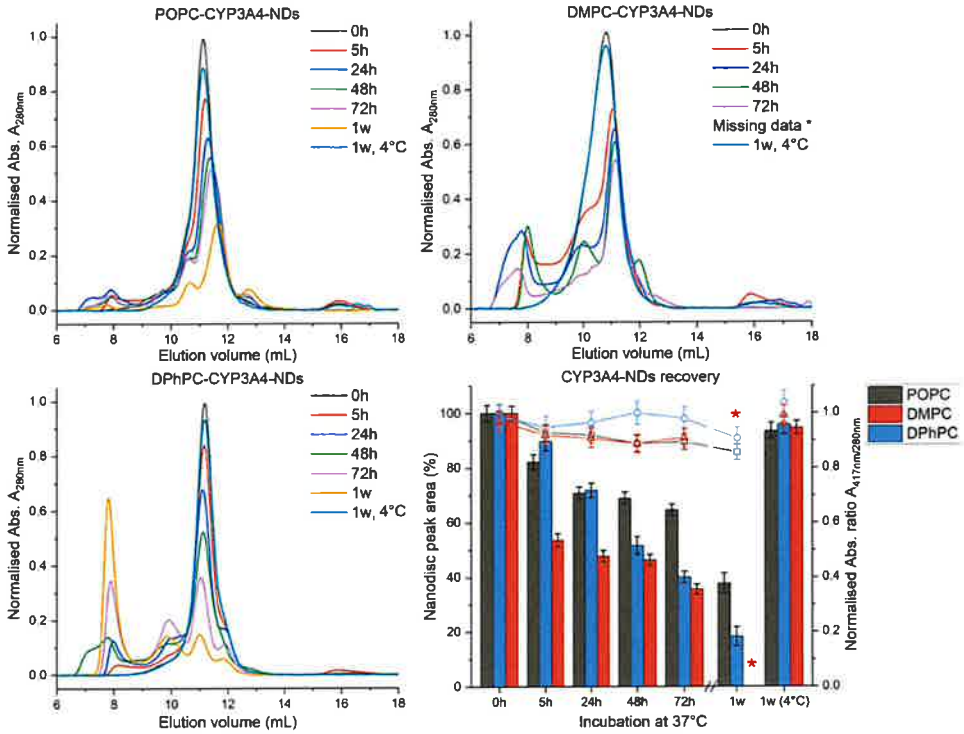

Fig. 10. Analytical SEC profiles (A_{280nm}) of CYP3A4-NDs formed with POPC, DMPC and DPhPC after incubation at 37 °C for 5 h up to a week. Each chromatogram was deconvoluted as shown in Fig. 9, and the relative fraction of the main CYP3A4-NDs peak area was quantified (bottom right panel). The normalised absorbance ratio between 417 nm (CYP3A4) and 280 nm (CYP3A4 + MSP1D1) is also shown, a constant ratio indicates that CYP3A4 remains present inside the ND. Error bars indicate two standard deviations of the mean peak surface area and absorbance ratios for duplicate measurements. The red asterisk indicates missing data.

hydrodynamic volumes. Furthermore, we have shown that ND lipid composition is not stable during incubation at elevated temperature for NDs comprising single linear alkyl chain lipids, because a portion of the lipid cargo is progressively lost during heating. In our hands, the T_m of CYP3A4 in aqueous solution was ~59 °C, which was comparable to CYP3A4 inside POPC and DMPC-NDs after correction for the presence of MSP1D1 and is similar to what others have reported for CYP3A4 in solution [34]. If our CD measurements are not corrected for the helicity of the MSPs, T_m values of ~4 °C higher are obtained, in line with the CD data of McClary and co-workers. CYP3A4 displayed a T_m of about 4 °C higher in DPhPC-NDs than in POPC and DMPC-NDs, indicating a difference in stability, which could be due to the lipid composition or presence of the third copy of MSP1D1.

We also demonstrate the use of SEC-MALS as a practical tool for the optimization of ND preparations and for determining the stability of membrane protein-incorporated NDs by assessing size distribution and composition as a function of temperature. Unfortunately, the thermostabilizing effects observed for saturated (phytanyl) lipids on empty NDs [27] did not translate well to CYP3A4-DPhPC-NDs. It appears that DPhPC-NDs were less stable with CYP3A4 incorporated, because the unfolding of CYP3A4 occurs before that of the MSPs, likely destabilising the complex. An important observation by McClary et al. was that the variation in T_m of CYP3A4-NDs could have been due to lipid packing differences, as they mention that the mixed POPC/DMPC CYP3A4-NDs, which conferred the highest stability to CYP3A4, were relatively lipid poor. In the present study, CYP3A4 was least stable in DMPC-NDs, and DMPC lipids were much more tightly packed in NDs than POPC and DPhPC, as is evident from the average lipid / ND contents measured by SEC-MALS, perhaps leaving less space available for CYP3A4 in the DMPC membrane. POPC is probably the most important lipid for the reconstitution of temperature sensitive membrane proteins, due to its low T_m, and DPhPC is similarly valuable because it is in a fluid crystalline state in a wide temperature range, and a high yield of CYP3A4-NDs could be achieved with DPhPC, demonstrating its potential application for the reconstitution of other instable membrane proteins.

3.2. Conclusions

NDs consisting of POPC or DMPC do not thermostabilize CYP3A4 relative to the soluble, aggregate form of this enzyme. In DPhPC-NDs, however, CYP3A4 exhibits a significantly higher melting temperature. This increase in stability does not translate to increased lifetime at 37 °C, unlike what was observed for DPhPC-NDs without an inserted membrane protein. The DPhPC ND is special, because it contains three, rather than the canonical two copies of MSP1D1. Also the branched nature of the isoprenoid lipids may confer specific properties to these NDs. The mixing of these fully saturated, rigid lipids with highly fluid lipids such as POPC or DPhPC could potentially yield a functional and stable membrane and would be an interesting strategy to pursue for the stabilization of proteins in NDs. However, mixed lipid ND composition and potential phase separation of the lipids will require careful monitoring.

4. Materials & methods

4.1. Storage and handling of lipids

Chemically synthetized lipids were bought from Avanti polar lipids. Lipid aliquots were stored at −20 °C as powder (saturated lipid) or chloroform/methanol ampules (unsaturated lipid). Lipids were taken directly from powder stocks into pre-weighed glass vials. Lipid in chloroform/methanol stocks were pipetted using Hamilton syringes into pre-weighed glass vials and dried under a gentle stream of nitrogen gas and kept overnight inside a vacuum chamber at <0.1 mPa. Lipid powder or films were weighed on a Sartorius Cubis® MCA6.6S-2S00-M

microbalance. This procedure was compared to total phosphorous concentration determination of the lipid stock solutions [35] and produced comparable and reproducible measures of the total lipid amounts.

4.2. Expression and purification of CYP3A4

The amino acid sequence for human CYP3A4 was obtained from the Uniprot online database, accession number P08684 and the gene encoding it was synthesized by GeneArt (Thermo Fisher Scientific). Previously, it was reported that an N-terminal truncation of amino acid residues 3–12 and a S18F substitution leads to increased CYP3A4 expression in *E. coli* [26,36]. The N-terminus of wild type CYP3A4 is MALIPDLAMETWLLLAVSLVLL..., and in this sequence the underlined residues were removed and at residue 18 (in bold) a Ser-to-Phe substitution was introduced [26]. The construct also included a C-terminal 6× histidine purification tag. The gene was amplified by PCR and cloned into the pET28a vector using *NdeI* and *XhoI* restriction enzymes. CYP3A4 was recombinantly expressed as described [23] with alterations; *E. coli* BL21(DE3) pLysS was transformed with the CYP3A4 (Δ3–12, S18F, 6-His) construct and the cells were incubated in terrific broth media supplemented with 50 μg / mL kanamycin, 34 μg / mL chloramphenicol and 1 mM thiamine in flat-bottom Erlenmeyer flasks at 37 °C, 200 rpm. Expression of the CYP3A4 gene was induced with 1 mM IPTG at $OD_{600} = 0.5$. At the time of induction, 4 g / L arabinose and 0.5 mM δ-aminolevulinic acid were added and the temperature was decreased to 30 °C, and the cells were harvested 40 h after induction. Cells harvested from 6 L were lysed by French press in buffer A (50 mM KPi, pH 7.4, 0.5 M KCl, 5 mM β-mercaptoethanol, 20 % glycerol) supplemented with cOmplete™, EDTA-free protease inhibitor tablet (Roche), 10 mg of DNase-I, ~50 mg lysozyme, in presence of 2 % (*w/v*) CHAPS detergent with a 5-fold excess of lysis buffer per gram of cell pellet (mL / g). After French press, the crude lysate was ultra-centrifuged at 45 k rpm in a 45 Ti rotor (Beckman Coulter). Imidazole (20 mM) was added to the supernatant and the pH readjusted to 7.4, after which the sample was loaded on a 5 mL TALON column (Cytiva) pre-equilibrated in buffer A, containing 20 mM imidazole and 0.5 % CHAPS on an NGC FPLC system (Bio-Rad) at 4 °C. The CYP3A4 bound to the column was washed extensively with up to 30 mM imidazole and was eluted with 300 mM imidazole. Finally, the protein was dialyzed to 3 × 1 L of storage buffer (50 mM KPi pH 7.4, 100 mM KCl, 20 % glycerol, 1 mM DTT), and 5 mM EDTA was added during the 1st buffer exchange, but during 2nd and 3rd exchange, EDTA was omitted to avoid interference with downstream IMAC purification steps during ND reconstitution. The concentration of CYP3A4 was determined (Fe^{2+} CO/Fe^{2+} difference spectra) according to the method of Omura and Sato [18], that was later elaborated by Geungerich and coworkers [19].

4.3. Nanodisc assembly procedures

MSP1D1 protein was expressed and purified as described previously [4,27]. His-tagged MSP1D1 was cleaved using Tobacco-etch virus (TEV) protease at a 1:50 molar ratio of TEV:MSP overnight and purified by reverse IMAC. Dried lipids were solubilized by addition of 100 mM sodium cholate stock solution. Sample vials were heated in warm tap water, vortexed and sonicated intermittently for approximately 45 min until the solution became completely transparent. MSP1D1 and CYP3A4 were added at the appropriate molar ratio determined for each of the lipids (Table 4). The reconstitution mixtures were prepared at a final concentration of 5 mM lipid and 20 mM cholate and left to equilibrate near the main phase transition temperature of the lipids for 1 h, DPhPC-NDs were equilibrated and assembled at 4 °C. The detergent was removed by 48 h dialysis at the respective equilibration temperatures in a 10 kDa MWCO slide-a-lyzer MINI dialysis tube (Thermo Fisher), containing 5 g amberlite bio-beads XAD-2 on the opposing side of the dialysis membrane. It was observed during previous experiments that direct contact with biobeads resulted in significant loss of protein and reduced ND yields by up to 50 %. The ND stoichiometric MSP1D1-to-lipid ratios were estimated by calculating the composition of a maximally filled ND by dividing the ND membrane surface area by the area per lipid. During the initial SEC purification, aggregated fractions, NDs and lipid poor fractions were identified by comparing to a gel filtration standard (Bio-Rad #1511901). The resulting lipid and protein composition of each fraction were analysed in detail by SEC-MALS and the MSP1D1-to-lipid ratio of the maximally filled ND was used for subsequent assembly experiments. A 5-fold excess of NDs over CYP3A4 was used with the same lipid-to-MSP1D1 ratio as for empty NDs. The concentrations of MSP1D1 and empty NDs were determined by absorbance spectroscopy at A_{280} using a theoretical extinction coefficient of $\varepsilon_{280} = 18{,}450\ M^{-1}\cdot cm^{-1}$ for MSP1D1(−his).

4.4. SEC-MALS protein conjugate analysis of NDs

Absolute Mw of empty and CYP3A4-NDs was measured using a SEC-MALS system comprising a miniDAWN® TREOS®, DynaPro®, Optilab differential refractometer (Wyatt technology) and 1260 Infinity II multiple wavelength absorbance detector (Agilent). The composition of empty NDs was determined using the protein conjugate method present in the ASTRA 8 software package. After selecting the peak area of interest and defining the $dn/dc_{protein}$, dn/dc_{lipid}, $\varepsilon_{280\ nm,\ protein}$ and $\varepsilon_{280\ nm,\ lipid}$, the Mw of the complex, the protein fraction and the conjugate "modifier" at each data slice throughout the peak selection are calculated. The program SEDFIT was used to calculate a theoretical dn/dc_{MSP1D1} of 0.188 mL/g and a weight averaged extinction coefficient of 0.869 $mg/mL^{-1}\cdot cm^{-1}$ at $\varepsilon_{280\ nm}$ for MSP1D1, based on its amino acid sequence [40]. A theoretical dn/dc_{lipid} of 0.16 mL/g was used for all lipids, and $\varepsilon_{280-417\ nm,\ lipid} = 0\ mg/mL^{-1}\cdot cm^{-1}$. The empty-ND MSP1D1-to-lipid ratios were determined by dividing the resulting protein and lipid Mw fractions by their respective molecular weights and calculating the ratio between the ND components. For CYP3A4 a dn/dc_{CYP3A4} of 0.187 was calculated. CYP3A4-NDs comprise three components; MSP1D1, CYP3A4 and lipids, as such the ND conjugate (lipids and MSPs) was regarded as the total "modifier", and depending on the lipid-to-MSP1D1 stoichiometry, $dn/dc_{Nanodisc}$ varies slightly. The dn/dc values of 0.169 (POPC-NDs), 0.168 (DMPC-NDs) and 0.174 (DPhPC-NDs) mL/g were calculated based on the compositions measured for empty NDs. A weight-averaged extinction coefficient of 1.387 $mg/mL^{-1}\cdot cm^{-1}$ at 417 nm for the aggregated CYP3A4 (in absence of detergent) was measured by SEC-MALS using a dRI detector to determine the concentration for the light scattering calculations. The resulting ε_{417nm} was lower than expected (~19 %), which can be explained the presence of apo CYP3A4

Table 4
Optimal reconstitution conditions determined for NDs assembled with different lipids.

Lipid abbreviation	Assembly ratio (Lipid/MSP1D1)	Assembly ratio MSP1D1/CYP3A4	ND assembly@temp. (°C)	Lipid theoretical@mass (Da)	Lipid main phase transition temp. T_m (°C)
POPC (16:0–18:1)	65	10	4	760	-2 [37]
DMPC (14:0)	80	10	25	678	24.1 [38]
DPhPC (4ME 16:0)	30	15[a]	4	846	None (−120 to 120) [39]

[a] DPhPC-NDs contain three copies of MSP1D1, so the ND ratios are adjusted accordingly.

or residual conjugated lipid or detergent from purification. Using the ε_{417nm}, dn/dc_{CYP3A4}, and $dn/dc_{nanodisc}$, the weight fraction of CYP3A4 and ND "modifier" were determined separately by protein-conjugate analysis. The Mw of the lipid fraction in CYP3A4-NDs was calculated by subtracting the theoretical $Mw_{MSP1D1(-his)}$ of 22 kDa per copy from the experimental $Mw_{Nanodisc}$ (44 kDa for POPC-NDs and DMPC-NDs, 66 kDa for DPhPC-NDs).

4.5. Circular dichroism spectroscopy

CD spectra were recorded using a JASCO J-815 spectropolarimeter, fitted with a Peltier temperature controller at a concentration of 4 μM CYP3A4, either free in solution or in NDs in 50 mM NaPi pH 7.4, 100 mM NaCl. During temperature scan experiments, residue ellipticity was measured at 222 nm at a ramp rate of 1 °C / min. The instrument was set to equilibrate to within 0.1 °C difference at each temperature increment. The raw CD data were baseline-corrected for the CD signal of buffer at 222 nm and where applicable for CYP3A4-NDs, the contribution of empty NDs comprising the same lipids, measured at the same concentration was subtracted. CD spectra were normalised from 0 to 1 and fitted with a Boltzmann sigmoidal function using OriginPro (OriginLab) to find the midpoint of the unfolding transition. The average apparent T_m is reported ± the standard error of the mean.

4.6. Differential scanning fluorimetry

NanoDSF measurements were performed on a Tycho (NanoTemper). Capillaries were loaded with 4 μM CYP3A4 either free in solution or in NDs, in 50 mM NaPi pH 7.4, 100 mM NaCl, and unfolding was measured from 35 to 95 °C for three to six replicates per sample, at a ramp rate of 30 °C per minute. The average T_m is reported ± two standard deviations of the mean. The Boltzmann fit produced the same T_m values within error as was obtained from the 1st derivative of the smoothed unfolding transition produced by the Tycho software package.

Supplementary data to this article can be found online at https://doi.org/10.1016/j.bbamem.2024.184372.

CRediT authorship contribution statement

Tim G.J. Knetsch: Writing – review & editing, Writing – original draft, Visualization, Methodology, Investigation, Formal analysis, Conceptualization. **Marcellus Ubbink:** Writing – review & editing, Validation, Supervision, Investigation, Funding acquisition, Conceptualization.

Declaration of competing interest

The project was funded by the Dutch Research Council with financial contributions from Batavia Biosciences B.V. and ZoBio B.V.

Data availability

Data will be made available on request.

Acknowledgements

The Dutch Research Council (NWO) is acknowledged for financial support of the project through the Applied and Engineering Sciences (AES), grant 16259 to MU. Dr. Abhinav Luthra and Dr. Maithili Krishnan-Schmieden are gratefully acknowledged for their advice on ND preparations.

References

[1] A. Jonas, Reconstitution of high-density lipoproteins, Methods Enzymol. 128 (1986) 553–582, https://doi.org/10.1016/0076-6879(86)28092-1.
[2] A. Jonas, J.H. Wald, K.L. Toohill, E.S. Krul, K.E. Kézdy, Apolipoprotein A-I structure and lipid properties in homogeneous, reconstituted spherical and discoidal high density lipoproteins, J. Biol. Chem. 265 (1990) 22123–22129, https://doi.org/10.1016/S0021-9258(18)45679-7.
[3] T.H. Bayburt, J.W. Carlson, S.G. Sligar, Reconstitution and imaging of a membrane protein in a nanometer-size phospholipid bilayer, J. Struct. Biol. 123 (1998) 37–44, https://doi.org/10.1006/jsbi.1998.4007.
[4] T.H. Bayburt, Y.V. Grinkova, S.G. Sligar, Self-assembly of discoidal phospholipid bilayer nanoparticles with membrane scaffold proteins, Nano Lett. 2 (2002) 853–856.
[5] T.K. Ritchie, Y.V. Grinkova, T.H. Bayburt, I.G. Denisov, J.K. Zolnerciks, W. M. Atkins, S.G. Sligar, Chapter 11 Reconstitution of Membrane Proteins in Phospholipid Bilayer Nanodiscs, Elsevier Masson SAS, 2009, https://doi.org/10.1016/S0076-6879(09)64011-8.
[6] T.H. Bayburt, S.G. Sligar, Membrane protein assembly into Nanodiscs, FEBS Lett. 584 (2010) 1721–1727, https://doi.org/10.1016/j.febslet.2009.10.024.
[7] J.E. Rouck, J.E. Krapf, J. Roy, H.C. Huff, A. Das, Recent advances in nanodisc technology for membrane protein studies (2012–2017), FEBS Lett. 591 (2017) 2057–2088, https://doi.org/10.1002/1873-3468.12706.
[8] I.G. Denisov, S.G. Sligar, Nanodiscs in membrane biochemistry and biophysics, Chem. Rev. 117 (2017) 4669–4713, https://doi.org/10.1021/acs.chemrev.6b00690.
[9] S.G. Sligar, I.G. Denisov, Nanodiscs: a toolkit for membrane protein science, Protein Sci. 30 (2021) 297–315, https://doi.org/10.1002/pro.3994.
[10] I.G. Denisov, S.G. Sligar, Nanodiscs for structural and functional studies of membrane proteins, Nat. Struct. Mol. Biol. 23 (2016) 481–486, https://doi.org/10.1038/nsmb.3195.
[11] J.H. Lin, A.Y.H. Lu, Interindividual variability in inhibition and induction of cytochrome P450 enzymes, Annu. Rev. Pharmacol. Toxicol. 41 (2001) 535–567, https://doi.org/10.1146/annurev.pharmtox.41.1.535.
[12] F.P. Guengerich, Cytochrome P450 and chemical toxicology, Chem. Res. Toxicol. 21 (2008) 70–83, https://doi.org/10.1021/tx700079z.
[13] M. Šrejber, V. Navrátilová, M. Paloncýová, V. Bazgier, K. Berka, P. Anzenbacher, M. Otyepka, Membrane-attached mammalian cytochromes P450: an overview of the membrane's effects on structure, drug binding, and interactions with redox partners, J. Inorg. Biochem. 183 (2018) 117–136, https://doi.org/10.1016/j.jinorgbio.2018.03.002.
[14] T. Zhang, J. Rao, W. Li, K. Wang, F. Qiu, Mechanism-based inactivation of cytochrome P450 enzymes by natural products based on metabolic activation, Drug Metab. Rev. 52 (2020) 501–530, https://doi.org/10.1080/03602532.2020.1828910.
[15] B.C. Monk, T.M. Tomasiak, M.V. Keniya, F.U. Huschmann, J.D.A. Tyndall, J. D. O'Connell, R.D. Cannon, J.G. McDonald, A. Rodriguez, J.S. Finer-Moore, R. M. Stroud, Architecture of a single membrane spanning cytochrome P450 suggests constraints that orient the catalytic domain relative to a bilayer, Proc. Natl. Acad. Sci. U. S. A. 111 (2014) 3865–3870, https://doi.org/10.1073/pnas.1324245111.
[16] N.A. Treuheit, M. Redhair, H. Kwon, W.D. McClary, M. Guttman, J.P. Sumida, W. M. Atkins, Membrane interactions, ligand-dependent dynamics, and stability of cytochrome P4503A4 in lipid nanodiscs, Biochemistry 55 (2016) 1058–1069, https://doi.org/10.1021/acs.biochem.6b00715.
[17] K. Berka, M. Paloncýová, P. Anzenbacher, M. Otyepka, Behavior of human cytochromes P450 on lipid membranes, J. Phys. Chem. B 117 (2013) 11556–11564, https://doi.org/10.1021/jp4059559.
[18] T. Omura, R. Sato, The carbon monoxide-binding pigment of liver Microsomes, J. Biol. Chem. 239 (1964) 2370–2378.
[19] F.P. Guengerich, M.V. Martin, C.D. Sohl, Q. Cheng, Measurement of cytochrome P450 and NADPH-cytochrome P450 reductase, Nat. Protoc. 4 (2009) 1245–1251, https://doi.org/10.1038/nprot.2009.121.
[20] P. Anzenbacher, J. Hudeček, R. Stružinský, Study of thermal stability of cytochrome P450 by differential scanning calorimetry, FEBS Lett. 149 (1982) 208–210, https://doi.org/10.1016/0014-5793(82)81102-2.
[21] L.B. Arendse, J.M. Blackburn, Effects of polymorphic variation on the thermostability of heterogenous populations of CYP3A4 and CYP2C9 enzymes in solution, Sci. Rep. 8 (2018) 1–14, https://doi.org/10.1038/s41598-018-30195-1.
[22] B.J. Baas, I.G. Denisov, S.G. Sligar, Homotropic cooperativity of monomeric cytochrome P450 3A4 in a nanoscale native bilayer environment, Arch. Biochem. Biophys. 430 (2004) 218–228, https://doi.org/10.1016/j.abb.2004.07.003.
[23] I.G. Denisov, Y.V. Grinkova, B.J. Baas, S.G. Sligar, The ferrous-dioxygen intermediate in human cytochrome P450 3A4: substrate dependence of formation and decay kinetics, J. Biol. Chem. 281 (2006) 23313–23318, https://doi.org/10.1074/jbc.M605511200.
[24] I.G. Denisov, B.J. Baas, Y.V. Grinkova, S.G. Sligar, Cooperativity in cytochrome P450 3A4: linkages in substrate binding, spin state, uncoupling, and product formation, J. Biol. Chem. 282 (2007) 7066–7076, https://doi.org/10.1074/jbc.M609589200.
[25] A. Nath, Y.V. Grinkova, S.G. Sligar, W.M. Atkins, Ligand binding to cytochrome P450 3A4 in phospholipid bilayer nanodiscs: the effect of model membranes, J. Biol. Chem. 282 (2007) 28309–28320, https://doi.org/10.1074/jbc.M703568200.
[26] W.D. McClary, J.P. Sumida, M. Scian, L. Paço, W.M. Atkins, Membrane fluidity modulates thermal stability and ligand binding of cytochrome P4503A4 in lipid nanodiscs, Biochemistry 55 (2016) 6258–6268, https://doi.org/10.1021/acs.biochem.6b00715.
[27] T.G.J. Knetsch, M. Ubbink, The effect of lipid composition on the thermal stability of nanodiscs, BBA-Biomembranes 1866 (2024) 184239, https://doi.org/10.1016/j.bbamem.2023.184239.

[28] G.B. Patel, G.D. Sprott, Archaeobacterial ether lipid liposomes (archaeosomes) as novel vaccine and drug delivery systems, Crit. Rev. Biotechnol. 19 (1999) 317–357, https://doi.org/10.1080/07388559991229170.
[29] Y. Koga, Thermal adaptation of the archaeal and bacterial lipid membranes, Archaea 2012 (2012), https://doi.org/10.1155/2012/789652.
[30] N. Skar-Gislinge, J.B. Simonsen, K. Mortensen, R. Feidenhans'l, S.G. Sligar, B. Lindberg Møller, T. Bjørnholm, L. Arleth, Elliptical structure of phospholipid bilayer nanodiscs encapsulated by scaffold proteins: casting the roles of the lipids and the protein, J. Am. Chem. Soc. 132 (2010) 13713–13722, https://doi.org/10.1021/ja1030613.
[31] I.G. Denisov, Y.V. Grinkova, A.A. Lazarides, S.G. Sligar, Directed self-assembly of monodisperse phospholipid bilayer Nanodiscs with controlled size, J. Am. Chem. Soc. 126 (2004) 3477–3487, https://doi.org/10.1021/ja0393574.
[32] M.T. Marty, H. Zhang, W. Cui, M.L. Gross, S.G. Sligar, Interpretation and deconvolution of nanodisc native mass spectra, J. Am. Soc. Mass Spectrom. 25 (2014) 269–277, https://doi.org/10.1007/s13361-013-0782-y.
[33] N. Skar-Gislinge, N.T. Johansen, R. Høiberg-Nielsen, L. Arleth, Comprehensive study of the self-assembly of phospholipid Nanodiscs: what determines their shape and stoichiometry? Langmuir 34 (2018) 12569–12582, https://doi.org/10.1021/acs.langmuir.8b01503.
[34] E.R. Samuels, I. Sevrioukova, Structure-activity relationships of rationally designed ritonavir analogues: impact of side-group stereochemistry, Headgroup spacing, and backbone composition on the interaction with CYP3A4, Biochemistry 58 (2019) 2077–2087, https://doi.org/10.1021/acs.biochem.9b00156.
[35] Avanti Polar Lipids, Determination of Total Phosphorus, 2022 https://avantilipids.com/tech-support/analytical-procedures/determination-of-total-phosphorus.
[36] E.M.J. Gillam, T. Baba, B.R. Kim, S. Ohmori, F.P. Guengerich, Expression of modified human cytochrome P450 3A4 in Escherichia coli and purification and reconstitution of the enzyme, archives of biochemistry and biophysics, Arch. Biochem. Biophys. 305 (1993) 123–131, https://doi.org/10.1006/abbi.1993.1401.
[37] D.R. Silvius, Thermotropic Phase Transitions of Pure Lipids in Model Membranes and their Modifications by Membrane Proteins, New York John Wiley Sons, Inc, 1982.
[38] R.N.A.H. Lewis, Y.P. Zhang, R.N. McElhaney, Calorimetric and spectroscopic studies of the phase behavior and organization of lipid bilayer model membranes composed of binary mixtures of dimyristoylphosphatidylcholine and dimyristoylphosphatidylglycerol, BBA-Biomembranes 1668 (2005) 203–214, https://doi.org/10.1016/j.bbamem.2004.12.007.
[39] H. Lindsey, N.O. Petersen, S.I. Chan, Physicochemical characterization of 1,2-diphytanoyl-sn-glycero-3-phosphocholine in model membrane systems, BBA-Biomembranes 555 (1979) 147–167, https://doi.org/10.1016/0005-2736(79)90079-8.
[40] H. Zhao, P.H. Brown, P. Schuck, On the distribution of protein refractive index increments, Biophys. J. 100 (2011) 2309–2317, https://doi.org/10.1016/j.bpj.2011.03.004.